INTERNATIONAL JOURNAL OF INNOVATIVE RESEARCH & DEVELOPMENT

ISSN 2278 – 0211 (Online)

Performance Analysis of Three Phase Induction Motor Drive Using SVPWM Switching Techniques: Design Approach

Manish Botkewar
Assistant Professor, Department of Electrical Engineering, Suresh Deshmukh College of Engineering, Wardha, India
KunalSawalakhe
Assistant Professor, Department of Electrical Engineering, Suresh Deshmukh College of Engineering, Wardha, India
Nikhil Wanjari
Assistant Professor, Department of Electrical Engineering, Suresh Deshmukh College of Engineering, Wardha, India

Abstract:
Space vector pulse width modulation (SVPWM) technique has emerged as a most used modulation strategy for the voltage source inverter (VSI) fed AC motor drives. Avoidance of the main spectral annoyance, harmonics concentration around the carrier frequency and it multiples, is done by increasing the switching frequency to a band which does not contribute mechanical vibrations and acoustic noises. This results in tremendous increase the switching losses. A systematic evaluation of SVPWM switching patterns can guide proper selection of switching frequency and vectors. A Matlab based comparative analysis of all these SVPWM variants in terms of attributes such as total harmonic distortion (THD) in output line voltage, DC bus utilization and the harmonic spread factor (HSF) is reported. For this using space vector pulse width modulation method a multilevel inverter above two level inverter can be designed. This simplification reduced considerably the computation time. A two level space vector pulse width modulation method also used for three as well as five level inverter.

Keywords:*Three-level inverter, triangle rotationol relations, SVPWM*

1. Introduction

Three phase dc/ac voltage source inverter (VSI) is used extensively in AC motor drives, active filters, and unified power flow controllers in power systems, and uninterrupted power supplies to generate controllable frequency and ac voltage magnitudes using various pulse width modulation (PWM) strategies. The PWM strategy plays an important role in the minimization harmonics and improving the fundamental in these inverters, especially in the three phase applications. Space vector pulse width modulation (SVPWM) technique has emerged as a most used modulation strategy for the voltage source inverter (VSI) fed AC motor drives. SVPWM is a method of pre-calculation of switching timing instants for various sections of target output which has options in terms of positioning vectors inside every sampling interval and has six possible patterns (variants) of the voltage vectors arrangements in each sector. SVPWM switching patterns, depending on the switching frequency, causes the mechanical vibration and the annoying acoustic noise to the drive system. Avoidance of the main spectral annoyance, harmonics concentration around the carrier frequency and it multiples, is done by increasing the switching frequency to a band which does not contribute mechanical vibrations and acoustic noises. This results in tremendous increase the switching losses. A systematic evaluation of SVPWM switching patterns can guide proper selection of switching frequency and vectors. A MATLAB based comparative analysis of all these SVPWM variants in terms of attributes such as total harmonic distortion (THD) in output line voltage and the DC bus utilisation is studied.

2. System Description, Functioning, Modeling, and theoretical Signals

2.1. Description

As shown on Fig. 1, the studied system is constituted of a DC supply, and a three-level voltage inverter bridge based on MOSFET's/Diodes pairs. Each arm contains four MOSFETs, four anti parallel diodes and two neutral clamping diodes.

2.2. Functioning

The three-level voltage inverter outputs three-level voltages (-E/2, 0, E/2) depending on the DC-bus voltage E and the variable state C_i, where 'i' is the phase indicator (i= a, b, c)

[6],[7]. *Si1*, *Si2*, *Si2'*, *Si1'* are the switches of one leg, and *Vio*is the phase-to-fictive middle point voltage. The functioning principle is displayed on Table 1. In order to obtain the desired three-level voltages, the converter must ensure complementarities between the pairs of switches: (*Si1,Si2'*) and (*Si2,Si1'*).

2.3. Modeling

For modelling, we follow the steps described in [7] and [8].

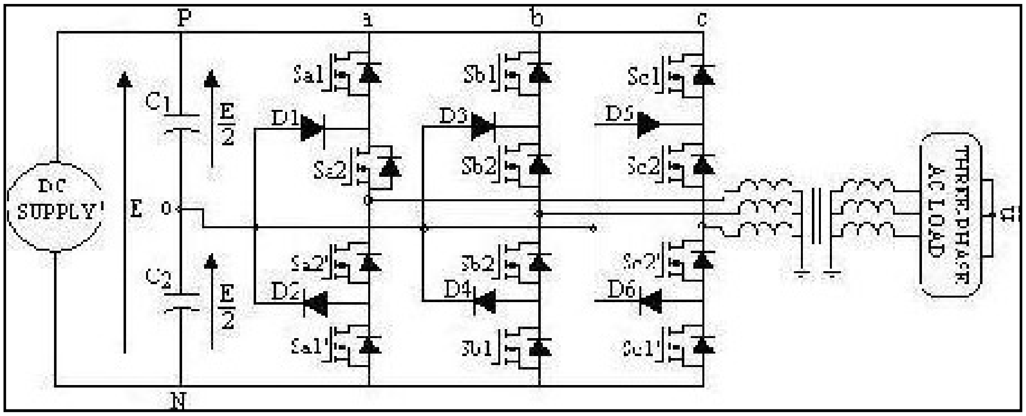

Figure 1: Three phase Three Level Inverter

Ci1	Si1	Si2	Si1'	Si2'	ViO
1	1	1	0	0	E/2
0	0	1	1	0	0
-1	0	0	1	1	-E/2

Table 1: Three Level Inverter Functioning Principal

*Vio*is linked to *E* through (1):

$Vio = Ci.(E / 2)$ (1)

The phase-to-neutral point voltage *Vin*depends on *Vio*via (2), (*i*= *a, b, c*):

$Vin = Vio - Vno$(2)

Assuming that the system is balanced, the sum of *Vin*is equal to zero:

$Van + Vbn + Vcn = 0$ (3)

Then, (2) and (3) end at:

$Vno = 1/3 \cdot (Vao + Vbo + Vco)$ (4)

By replacing *Vno*in (2), we obtain the following system:

$$\begin{bmatrix} Van \\ Vbn \\ Vcn \end{bmatrix} = \begin{bmatrix} 2/3 & -1/3 & -1/3 \\ -1/3 & 2/3 & -1/3 \\ -1/3 & -1/3 & 2/3 \end{bmatrix} \begin{bmatrix} Vao \\ Vbo \\ Vco \end{bmatrix} \quad (5)$$

Let now apply the Concordia transformation to the vector *Vin*giving it in the diphase (α-β) frame:

$$\begin{bmatrix} V\alpha \\ V\beta \end{bmatrix} = \sqrt{\frac{2}{3}} \begin{bmatrix} 1 & \frac{-1}{2} & \frac{-1}{2} \\ 0 & \frac{\sqrt{3}}{2} & \frac{\sqrt{3}}{2} \end{bmatrix} \begin{bmatrix} Van \\ Vbn \\ Vcn \end{bmatrix} \quad (6)$$

Now, considering the 'm' states (m = 1, 0, -1) of the variable

Ci, we obtain the '*mq*' possible combination of the three-level voltage inverter ('*q*' is the phase number, here *q* = 3). The result is 27 vectors grouped in Table 2, where we notice that there are 03 zero vectors *(V*0*, V*7*, V*14), and a group of 12vectors representing in pairs the same coordinates (α-β):

(*V*11,*V*12) , (*V*21,*V*22), (*V*31,*V*32), (*V*41,*V*42), (*V*51,*V*52), and(*V*61,*V*62). By drawing these 27 vectors in the (α-β) frame, as illustrated on Fig. 2, we can distinguish between the three hexagons displayed on Fig. 3:

- *The small hexagon* (Fig.3.a), defined by the six regions I, II,III, IV, V, and VI. All vectors limiting these regions have the same magnitude: *E*/√6.

The middle hexagon (Fig.3.b), defined by the six regions a,
b, c, d, e, and f. All vectors limiting these regions have the same magnitude: *E*/√2.

The big hexagon (Fig.3.c), defined by the six regions A, B,
C, D, E, and F. All vectors limiting these regions have the same magnitude: *E*.(√2/√3).

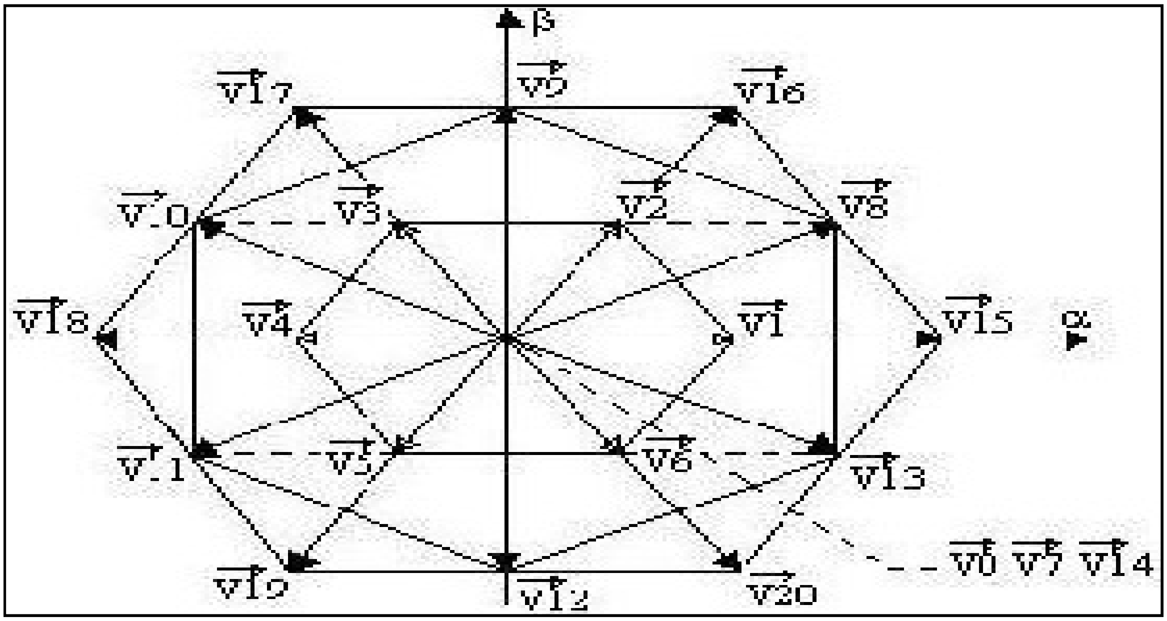

Figure 2: Three level inverters in the (α-β) frame

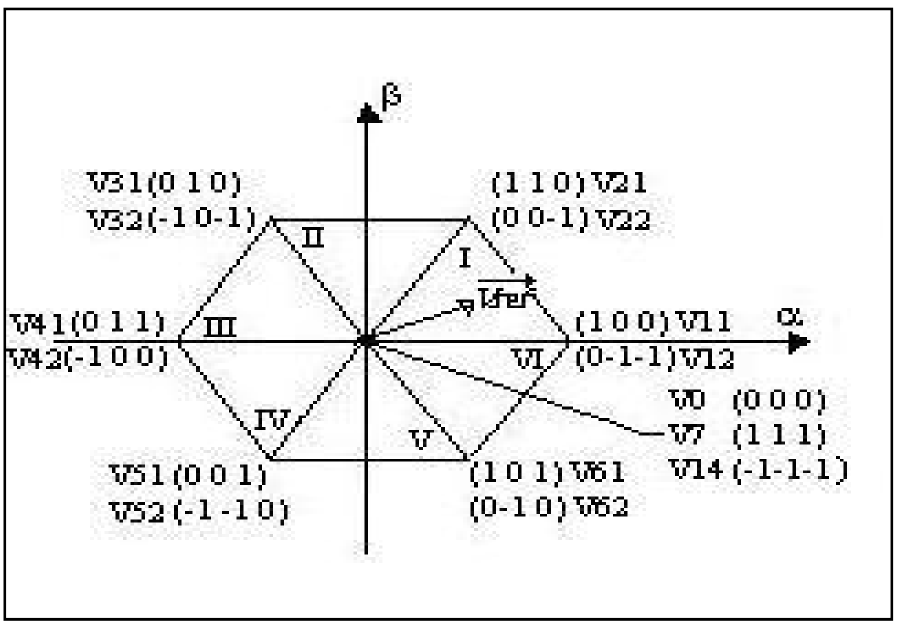

Figure 3(a): Small hexagon

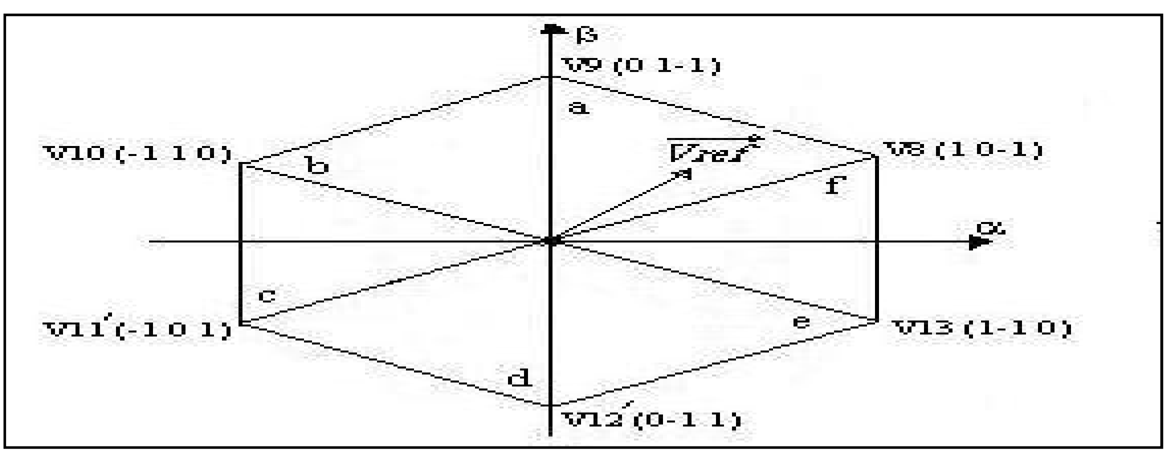

Figure 3(b): Middle hexagon

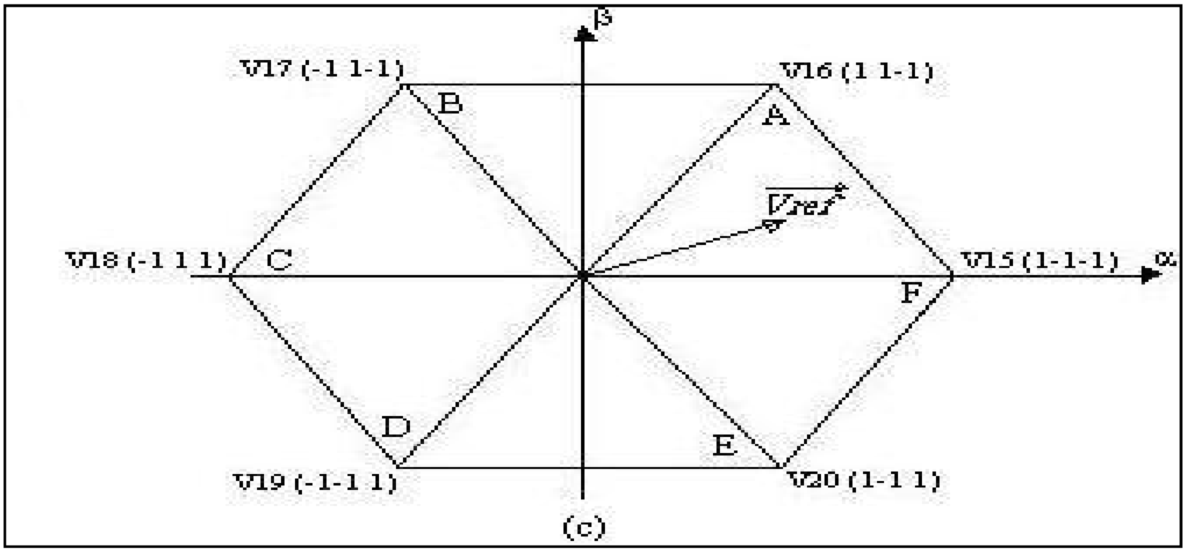

Figure 3 (c): Big hexagon

2.4. Theoretical Signals

According to [9], the theoretical signals that outputs the Three-level voltage inverter, representing *Vio*and *Vin* respectively, are as displayed on Figure4 (case of phase a). Here, we can see three voltage levels on *Vao*: -E/2, 0, and E/2, and three voltage levels on *Van*: E/3, E/2, and 2E/3.

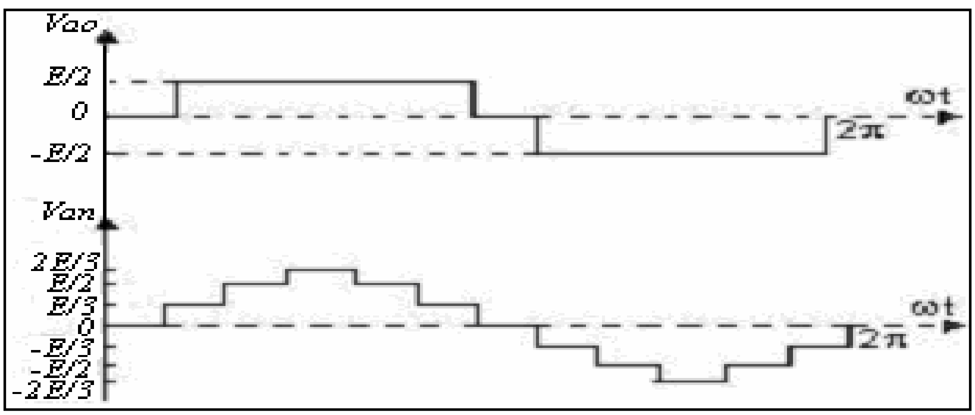

Figure 4 :Theoretical voltages of the three-level inverter

3. Inverter's Gating Signals Generation

Several strategies are proposed in order to generate the inverter’s gates pulses. In this work, we used the space vector modulation SVPWM, which is a kind of the pulse width modulation PWM strategies [8], [10].

In this topic, the principle and the description of the SVPWM strategy will be detailed and applied to the three level voltage inverter in an open loop functioning.

3.1. Principle

As shown on Fig. 3, in each of the three hexagons, the reference vector *V*ref is located in one of the six regions constituting the hexagon, where each region is limited by two adjacent vectors *V*δet *V*δ+1 (Figure 5). Then *V*ref is equal to

$$\vec{V}_{ref} = \frac{T_\delta}{Ts}\vec{V}\delta + \frac{T_{\delta+1}}{Ts}\vec{V}_{\delta+1} \qquad (7)$$

*T*s is the sampling time, *T*δ, *T*δ*+1* are the application times of *V*δ and *V*δ*+1* respectively. In one sample time, *V*ref is equal to *V*δ during *T*δ and *V*δ*+1* during *T*δ*+1*. In the rest of *T*s, *V*ref is equal to the zero vectors (*V*14, *V*0, and *V7*) during *T*0 following this optional choice: *V*14, *V*0 at the pulse’s ends and *V*7 at the pulse’s centre. At the same time:

$$\vec{V}_{ref} = \vec{V}_{ref\alpha} + \vec{V}_{ref\beta} \qquad (8)$$

Or, in complex writing

$$\overline{V}_{ref} = \sqrt{V_{ref\,\alpha}^{\;\;2} + V_{ref\,\beta}^{\;\;2}}\,.e^{\,j(\varphi - \pi/2)} \qquad (9)$$

Where ϕ is an angle varying from 0 to 2π.
Then,

$$T_0 = T_S - T_\delta - T_{\delta+1} \qquad (10)$$

The SVPWM pulse is a pulse which is symmetrical and where all switches of the inverter's half-bridge have the samestate in the centre and in the two ends. So, following these properties and after calculation of $T\delta$,$T\delta+1$ and $T0$ of each region belonging to the appropriate hexagon, we arrive to build the pulses of the higher half-bridge (*Si1*, *Si2*, *i = a, b, c*, with *Si2'*, *Si1'* as respective complementarities) of the three level inverter.

3.2. Switching Times Calculation

As said previously, we distinguish between 03 hexagons(Fig. 3), where each one is constituted of 06 regions. As a result, we have 18 regions that wait the calculation of the irrespective switching times. To simplify this task, and for reason of similarities in the 06 regions of one hexagon on the one hand, and resemblance between hexagons 'a' and 'c' on the other hand (the largest magnitude in hexagon 'a' ($E/\sqrt{6}$) constitutes the half of the largest magnitude in hexagon 'c'($E.\sqrt{2}/\sqrt{3}$)), for these all reasons, in the switching times calculation's procedure presentation, only two regions of hexagon 'a' and hexagon 'b', corresponding to the positive components of *Vref*, will be considered (Fig. 4). The other switching times will be then deduced from these four regions. Remind-we that the limiting vectors (*V1* to *V20*) magnitudes will take the following values:

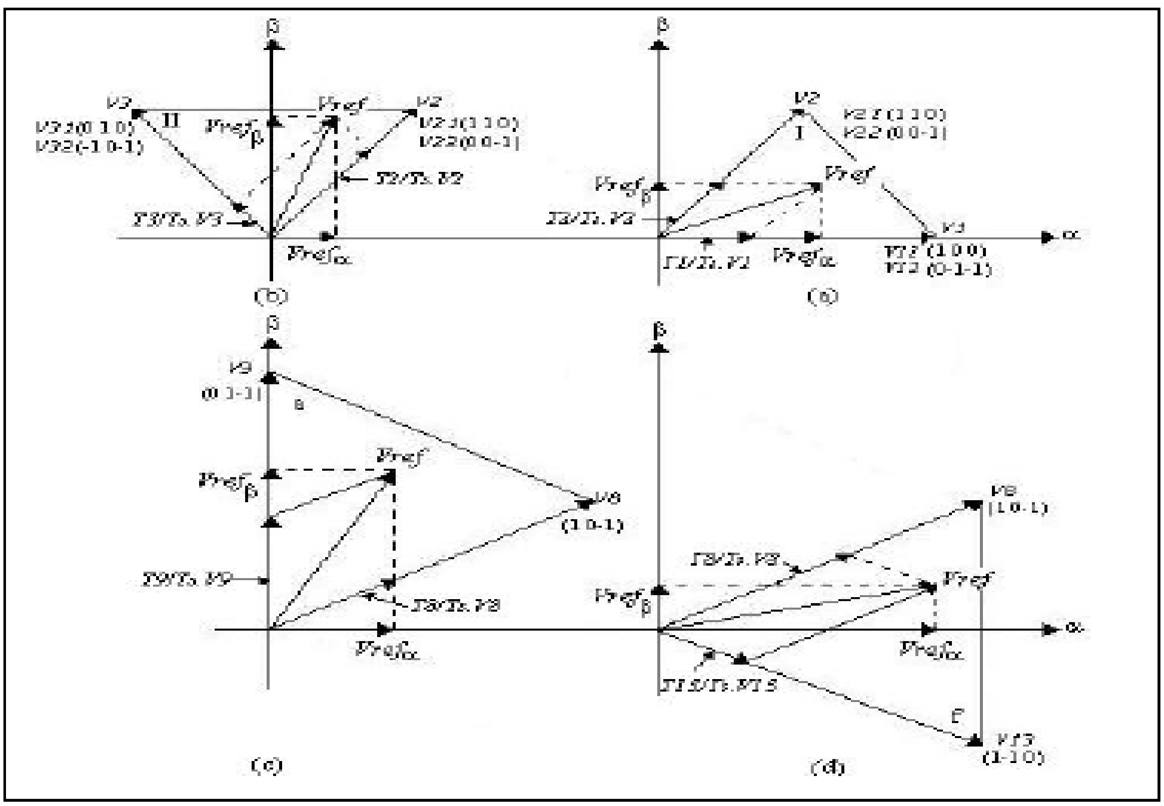

Figure 5: Switching times calculation

V_1 to $V_6 \rightarrow E/\sqrt{6}$, V_8 to $V_{13} \rightarrow E/\sqrt{2}$, V_{15} to $V_{20} \rightarrow E.(\sqrt{2}/\sqrt{3})$.
$V_7 = V_{14} = V0 = 0$.

- *Region I* (Fig.6.a) switching times calculation:

$$V_{ref\alpha} = (T_1 / T_S).V_1 + (T_2 / T_S).V_2.\sin(\pi / 6) \tag{11}$$

$$V_{ref\beta} = (T_2 / T_S).V_2.\cos(\pi / 6) \tag{12}$$

$$T_1 = \frac{\sqrt{6}\,Vref\alpha - \sqrt{2}\,Vref\beta}{E}.Ts \tag{13}$$

$$T_2 = \frac{2\sqrt{2}\,Vref\beta}{E}.Ts \tag{14}$$

- *Region II* (Fig.6.b) switching times calculation:

$$V_{ref\alpha} = ((T_2 / T_S).V_2 - (T_3 / T_S).V_3).\sin(\pi / 6) \tag{15}$$

$$V_{ref\beta} = ((T_2 / T_S).V_2 + (T_3 / T_S).V_3).\cos(\pi / 6) \tag{16}$$

$$T_2 = \frac{\sqrt{6}\,Vref\alpha + \sqrt{2}\,Vref\beta}{E}.Ts \tag{17}$$

$$T_3 = \frac{-\sqrt{6}\,Vref\alpha + \sqrt{2}\,Vref\beta}{E}.Ts \tag{18}$$

- *Region a* (Fig.6.c) switching times calculation:

$$V_{ref\alpha} = (T_8 / T_S).V_8.\cos(\pi / 6) \tag{19}$$

$$V_{ref\beta} = (T_8 / T_S).V_8.\sin(\pi / 6) + T_9 / T_S.V_9 \tag{20}$$

$$T_8 = \frac{2\sqrt{2}\,Vref\alpha}{\sqrt{3}\,E}.Ts \tag{21}$$

$$T_9 = \frac{\sqrt{6}\,Vref\beta - \sqrt{2}\,Vref\alpha}{\sqrt{3}\,E}.Ts \tag{22}$$

- *Region f* (Fig.6.d) switching times calculation:

$$V_{ref\alpha} = ((T_8 / T_S).V_8 + (T_{13} / T_S).V_{13}).\cos(\pi / 6) \tag{23}$$

$$V_{ref\beta} = ((T_8 / T_S).V_8 - (T_{13} / T_S).V_{13}).\sin(\pi / 6) \tag{24}$$

$$T_8 = \frac{\sqrt{6}\,Vref\beta + \sqrt{2}\,Vref\alpha}{\sqrt{3}\,E}.Ts \tag{25}$$

$$T_{13} = \frac{-\sqrt{6}\,Vref\beta + \sqrt{2}\,Vref\alpha}{\sqrt{3}\,E}.Ts \tag{26}$$

3.3. Examples of Chronograms
below are illustrated the pulses of regions 'i' and 'a' in Figure 7.a and Figure 7.b respectively, where we can see a symmetrical signals that have the same states at the center and at the ends.
note that $t11 = t12 = t1/2$, and $t21 = t22 = t2/2$.
then the zero voltage time application is given by:
$t0 = (ts - t\delta - t\delta + 1) / 6$ (27)
where,
$t\delta$, $t\delta+1$: times of $v\delta$ and $v\delta+1$.
D. Hexagons transition condition
the transition from a hexagon to the two others is function of the reference vector $v$ref. this last depends on the largest magnitude of each hexagon. we have:

- if ($-e/\sqrt{6} \leq v$ref$\leq e/\sqrt{6}$) $\Rightarrow$vref belongs to one of the six regions of the small hexagon ‘a’.
- if ($-e/\sqrt{2} \leq v$ref$\leq e/\sqrt{2}$) $\Rightarrow$vref belongs to one of the six regions of the middle hexagon ‘b’.
- if ($-e.\sqrt{2}/\sqrt{3} \leq vref\leq e.\sqrt{2}/\sqrt{3}$) $\Rightarrow$vref belongs to one of the six regions of the big hexagon ‘c’

4. Main Circuit and Simulation Results

4.1. Main Circuit

Figure 9 shows the overalls imulation model of three-level inverter. Matlab/simulink simulation software issued to build three-level inverter SVPWM control simulation model, which based on the improved traditional three-level inverter SVPWM algorithm. Direct-current supply voltage E =600V, Simulation sampling time T_S = 0.0004 s

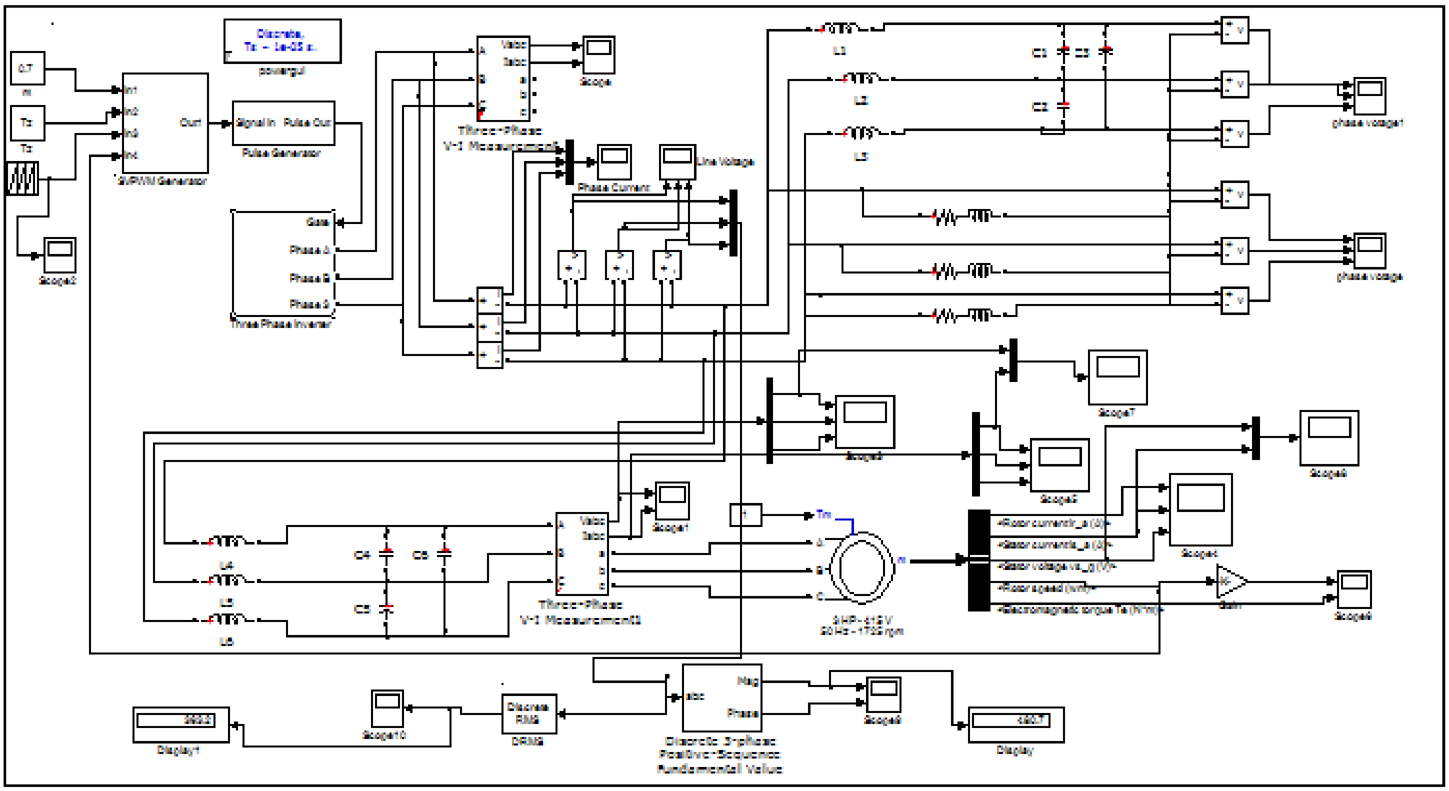

Figure 6: simulation model of three level inverter fed IM

4.2. Simulation Results

Simulation were carried out for constant v/f control of induction motor drives using SPWM techniques for closed loop system. The parameters of the induction motor used for simulation are as follows:

220V, 50Hz, 2pole, 3hp

Rs=0.432Ω, Ls=4mH

Rr=0.816Ω, Lr=2mH, Lm=69mH

J=0.089KG-M2, B=.0, TL=10.32N-m;

The inverter switching frequency is 2.1 kHz the D.C link voltage is 300Vand the modulation index is 0.7

Figure 10 show the output phase voltages of SVM inverter , Figure 11 shows the stator current and stator voltage , Figure 12 shows the speed of IM and the torque developed and Fig 13

Shows the THD analysis of the stator current with close loop control. It can be observed that speed of the induction motor is increased with SVM for same D.C input voltageThe circuit system becomes simple and easy to operate by using the improved SVPWM method. From the simulation results, it can also be found that the load side current wave form derived from the simplified SVPWM method is better. Without filter, THD is smaller than 4 %, it meets the

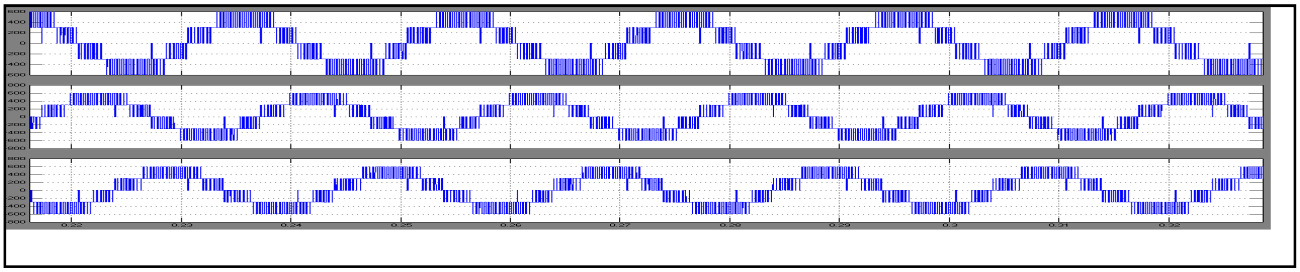

Figure 7: Output phase voltages of SVM inverter

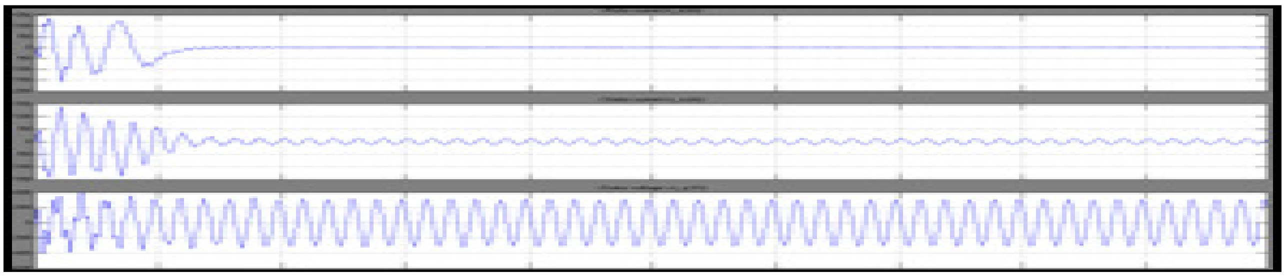

Figure 8: Simulation result of rotor current, stator current and stator voltage

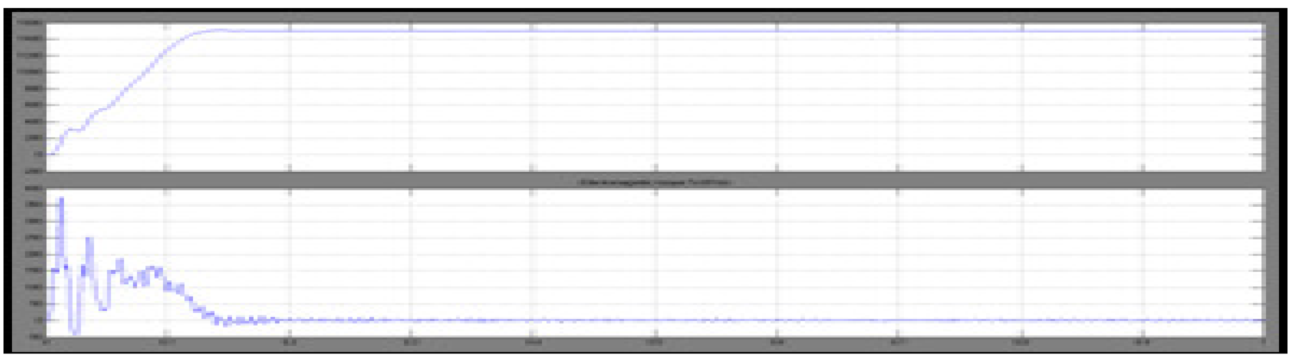

Figure 9: simulation result of speed and electromagnetic toque

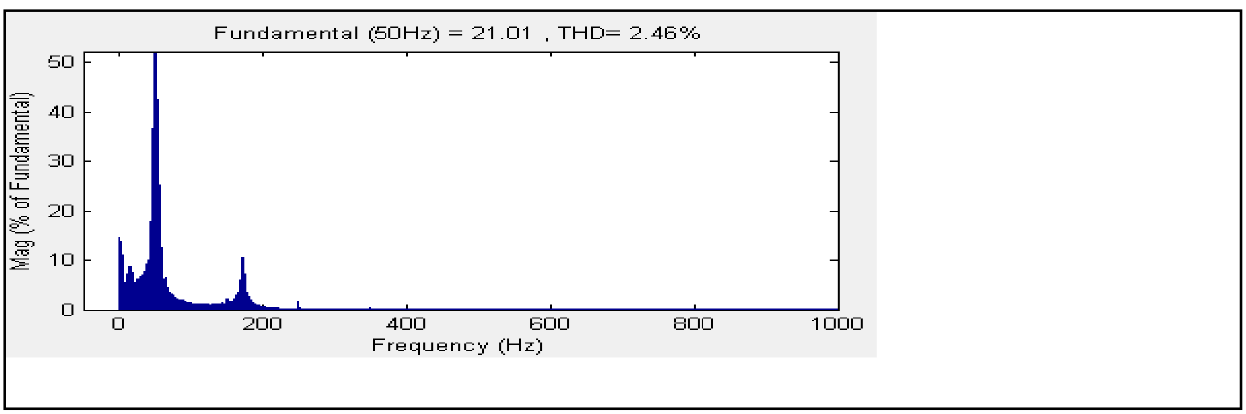

Figure 10: THD of Stator Current

5. Conclusion

The Matlab based comparative analysis of SVPWM variants in terms of attributes such as total harmonic distortion (THD) in output line voltage, DC bus utilization and the harmonic spread factor (HSF). To realize such analysis of these attributes using space vector pulse width modulation method a multilevel inverter above two level inverter will be designed. This will simplify and reduce the computation time considerably. A two level space vector pulse width modulation method may also be used for three as well as five level inverter.

6. References

i. DrazenDujic, Martin Jones, Emil Levi, Joel Prieto , and Federico Barrero "Switching Ripple Characteristics of Space Vector PWM schemes for Five-Phase Two-Level Voltage Source Inverters—Part 1: Flux Harmonic Distortion Factors " IEEE TRANSACTIONS ON INDUSTRIAL ELECTRONICS, VOL. 58, NO. 7, pp. 2789-2798, JULY 2011.

ii. Behrooz Mirafzal, Mahdi Saghaleini, and Ali Kashefi Kaviani "An SVPWM-Based Switching Pattern for Stand-Alone and Grid-Connected Three-Phase Single-Stage Boost Inverters" IEEE TRANSACTIONS ON POWER ELECTRONICS, VOL. 26, NO. 4,pp. 1102-1111, APRIL 2011.

iii. Guo-Ming Sung, Chih-Ping Yu, Tsai-Wang Hung, and Hsiang-Yuan Hsieh "Mixed-Mode Chip Implementation of Digital Space SVPWM With Simplified-CPU and 12-Bit 2.56 Ms/s Switched-Current Delta-Sigma ADC in Motor Drive" IEEE TRANSACTIONS ON POWER ELECTRONICS, VOL. 27, NO. 2, pp. 916-930, FEBRUARY 2012.

iv. Sanbo Pan, Junmin Pan, and Zuohua Tian "A Shifted SVPWM Method to Control DC-Link Resonant Inverters and Its FPGA Realization" IEEE TRANSACTIONS ON INDUSTRIAL ELECTRONICS, VOL. 59, NO. 9, pp. 3383-3391, SEPTEMBER 2012

v. Changliang Xia, Hongjun Shao, Yun Zhang, and Xiangning He "Adjustable Proportional Hybrid SVPWM Strategy for Neutral-Point-Clamped Three-Level Inverters" IEEE TRANSACTIONS ON INDUSTRIAL ELECTRONICS, VOL. 60, NO. 10, pp. 4234-4242 OCTOBER 2013.

vi. Mario J. Durán, Joel Prieto, Federico Barrero, José A. Riveros, and Hugo Guzman "Space-Vector PWM With Reduced Common-ModeVoltage for Five-Phase Induction Motor Drives " IEEE TRANSACTIONS ON INDUSTRIAL ELECTRONICS, VOL. 60, NO. 10, pp. 4159-4168 OCTOBER 2013.

vii. Guojun Tan, Qingwei Deng, and Zhan Liu "An Optimized SVPWM Strategy for Five-LevelActive NPC (5L-ANPC) Converter" IEEE TRANSACTIONS ON POWER ELECTRONICS, VOL. 29, NO. 1, pp. 386-395, JANUARY 2014.

viii. Wenyi Liang, Jianfeng Wang, Patrick Chi-Kwong Luk, Weizhong Fang, and Weizhong Fei"Analytical Modeling of Current Harmonic Components in PMSM Drive With Voltage-SourceInverter by SVPWM Technique" IEEE TRANSACTIONS ON ENERGY CONVERSION, VOL. 29, NO. 3, pp. 673-680, SEPTEMBER 2014.

ix. Qun-tao An, M.H. Duan, L. Sun and G.L. Wang "SVPWM strategy of post-fault reconfigured dual inverter in open-end winding motor drive systems" ELECTRONICS LETTERS 14th August 2014 Vol. 50 No. 17 pp. 1238–1240.

x. Chaurasiya Rohit B.,Mukesh D.Patil,Divya Shah,Abhijit Kadam "FPGA Implementation of SVPWM Control Technique for Three Phase Induction Motor Drive Using Fixed Point Realization "Proceeding Of IEEE International Conference on Circuits, Systems, Communication and Information Technology Applications (CSCITA), pp.651-656,2012.